PHYSICAL REVIEW D **96,** 055004 (2017)

Naturalness and dark matter in the supersymmetric $B-L$ extension of the standard model

Luigi Delle Rose,[1,2] Shaaban Khalil,[3] Simon J. D. King,[1] Carlo Marzo,[4] Stefano Moretti,[1,2] and Cem S. Un[5]

[1]*School of Physics and Astronomy, University of Southampton, Highfield, Southampton SO17 1BJ, United Kingdom*

[2]*Particle Physics Department, Rutherford Appleton Laboratory, Chilton, Didcot, Oxon OX11 0QX, United Kingdom*

[3]*Center for Fundamental Physics, Zewail City of Science and Technology, Sheikh Zayed, 12588 Giza, Egypt*

[4]*National Institute of Chemical Physics and Biophysics, Rävala 10, 10143 Tallinn, Estonia*

[5]*Department of Physics, Uludağ University, TR16059 Bursa, Turkey*

(Received 30 May 2017; published 6 September 2017)

We study the naturalness properties of the $B-L$ supersymmetric standard model (BLSSM) with type-I seesaw and compare them to those of the minimal supersymmetric standard model (MSSM) at both low (i.e., Large Hadron Collider) energies and high (i.e., unification) scales. By adopting standard measures of naturalness, we assess that, in the presence of full unification of the additional gauge couplings and scalar/fermionic masses of the BLSSM, such a scenario reveals a somewhat higher degree of fine-tuning (FT) than the MSSM, when the latter is computed at the unification scale and all available theoretical and experimental constraints, but the dark matter (DM) ones, are taken into account. Yet, such a difference, driven primarily by the collider limits requiring a high mass for the gauge boson associated to the breaking of the additional $U(1)_{B-L}$ gauge group of the BLSSM in addition to the $SU(3)_C \times SU(2)_L \times U(1)_Y$ of the MSSM, should be regarded as a modest price to pay for the former in relation to the latter, if one notices that the nonminimal scenario offers a significant volume of parameter space where numerous DM solutions of different compositions can be found to the relic density constraints, unlike the case of the minimal structure, wherein only one type of solution is accessible over an ever diminishing parameter space. In fact, this different level of tension within the two SUSY models in complying with current data is well revealed when the FT measure is recomputed in terms of the low-energy spectra of the two models, over their allowed regions of parameter space now in the presence of all DM bounds, as it is shown that the tendency is now opposite, with the BLSSM appearing more natural than the MSSM.

DOI: 10.1103/PhysRevD.96.055004

I. INTRODUCTION

Low-scale supersymmetry (SUSY) is motivated by solving two major flaws of the standard model (SM): the gauge hierarchy and dark matter (DM) problems.

In the SM, the hierarchy problem stems from the fact that a very unnatural fine-tuning (FT) is required to keep the Higgs mass at an acceptable value for current data. SUSY provides an elegant solution to this. However, SUSY must be broken at a high scale, hence some FT is reintroduced at some level. In the minimal supersymmetric standard model (MSSM), with universal soft SUSY breaking terms, a heavy spectrum is required to give large radiative corrections to the SM-like Higgs mass and account for the recently measured value of 125 GeV at the Large Hadron Collider (LHC). Thus naturalness becomes seriously challenged in the MSSM by well established experimental conditions.

Furthermore, the alluring hints of DM existence are serious indications for new physics Beyond the SM (BSM). Due to R-parity conservation, the lightest SUSY particle (LSP) in the MSSM, the lightest neutralino, is stable and thus is a good candidate for DM. However, in the constrained MSSM (CMSSM) framework, in which universal boundary conditions are imposed at the grand unification theory (GUT) scale, the extra Higgs bosons of the MSSM are beyond the reach of the LHC experiments, while the lightest CP-even Higgs boson is reserved as the SM-like one. Such heavy Higgs bosons result in large fine-tuning at the Electro-Weak (EW) scale. In addition, the strict bound on the gluino mass ($m_{\tilde{g}} \leq 1.9$ TeV [1]) causes heavy EW-inos (bino and wino) at low scale, since the gaugino masses are also set universal at the GUT scale. Besides, the null results from direct searches for SUSY particles lead to a heavy mass spectrum. The ensuing EW sector, in particular, severely raises the required FT leading to the correct scale for EW symmetry breaking (EWSB). Even though it is not possible to exclude the CMSSM completely, such a heavy spectrum brings poor agreement with various precision observables [2]. Detailed discussions of the FT issue in the CMSSM framework can be found in [3].

*L.Delle-Rose@soton.ac.uk
†Skhalil@zewailcity.edu.eg
‡SJD.King@soton.ac.uk
§Carlo.Marzo@kbfi.ee
‖S.Moretti@soton.ac.uk
¶cemsalihun@uludag.edu.tr

Besides the LHC ones, the latest measurements for DM also provide strict constraints for the MSSM regardless of imposing universal boundary conditions at the GUT scale or otherwise. The latest results from, e.g., the LUX Collaboration [4] have a strong impact especially for light DM candidates. A low FT condition requires the Higgsino-like LSP neutralino to have a large cross section with nuclei, since the relevant scattering processes happen through the Yukawa interactions, so that LUX results exclude such solutions. Indeed, only a binolike LSP neutralino can more or less survive, since its corresponding scattering cross section is instead low [5]. However, the relic abundance of the bino is usually much larger than the ranges allowed by the current Wilkinson Microwave Anisotropy Probe (WMAP) and Planck results [6,7].

Quite apart from the aforementioned two problems of the SM, it should be recalled that nonvanishing neutrino masses are presently some of the most important evidence for BSM physics. Massive neutrinos are not present in the SM. However, a simple extension of it, based on the gauge group $SU(3)_C \times SU(2)_L \times U(1)_Y \times U(1)_{B-L}$, can account for current experimental results of light neutrino masses and their large mixing [8–18]. Within the $B-L$ supersymmetric standard model (BLSSM), the SUSY version of such a scenario, which inherits the same beneficial features of the MSSM in connection with SUSY dynamics, it has been emphasized that the scale of $B-L$ symmetry breaking is related to the SUSY breaking one and both occur in the TeV region [19–24]. Therefore, several testable signals of the BLSSM are predicted for the current experiments at the LHC [25–36].

In addition, the BLSSM provides new candidates for DM different from those of the MSSM. In particular, there are two kinds of neutralinos, corresponding to the gaugino of $U(1)_{B-L}$ and the $B-L$ Higgsinos. Also a right-handed sneutrino, in a particular region of parameter space, may be a plausible candidate for DM. We also consider the scenario where the extra $B-L$ neutralinos can be cold DM states. We then examine the thermal relic abundance of these particles and discuss the constraints imposed on the BLSSM parameter space from the negative results of their direct detection. We argue that, unlike the MSSM, the BLSSM offers one with significant parameter space satisfying all available experimental constraints. This may be at the expense of high FT, if Z' is quite heavy and soft SUSY breaking terms are universal. Nevertheless, for what we will eventually verify to be a small increase in FT with respect to the MSSM, we will gain in the BLSSM a more varied DM sector and much better compliance with relic and (in)direct detection data.

In the buildup to this DM phenomenology, we analyze the naturalness problem in the BLSSM and compare its performance in this respect against that of the MSSM. In the latter, the weak scale (M_Z) depends on the soft SUSY breaking terms through the renormalization group equations (RGEs) and the EW minimization conditions, which can be expressed as

$$\frac{1}{2}M_Z^2 = \frac{m_{H_d}^2 - m_{H_u}^2 \tan^2\beta}{\tan^2\beta - 1} - \mu^2. \tag{1.1}$$

Therefore, a possible measure of FT is defined as [37]

$$\Delta(M_Z^2, a) = \left| \frac{a}{M_Z^2} \frac{\partial M_Z^2}{\partial a} \right|, \tag{1.2}$$

where a stands for the GUT-scale parameters (e.g., m_0, $m_{1/2}, A_0$, etc.) or low-scale parameters (e.g., M_1, M_2, M_3, $m_{\tilde{q}}, m_{\tilde{\ell}}$, etc.). In order for SUSY to stabilize the weak scale, $\Delta \equiv \mathrm{Max}(\Delta(M_Z^2, a))$ should be less than $\mathcal{O}(100)$. However, as the scale of SUSY breaking is increased, the EW one becomes highly fine-tuned. As intimated, in the BLSSM, both the weak and $B-L$ scales are related to soft SUSY breaking terms and, in addition to Eq. (1.1), which is slightly modified by the presence of the gauge mixing $\tilde{g}$, we also have, in the same limit $\tilde{g} \simeq 0$,

$$\frac{1}{2}M_{Z'}^2 = \frac{m_{\eta_1}^2 \tan^2\beta' - m_{\eta_2}^2}{1 - \tan^2\beta'} - \mu'^2, \tag{1.3}$$

where $\eta_{1,2}$ are scalar bosons, with $\langle \eta_{1,2} \rangle = v'_{1,2}$ that break the $B-L$ symmetry spontaneously, and $\tan\beta' = v'_1/v'_2$. The bound on $M_{Z'}$, due to negative searches at LEP, is given by $M_{Z'}/g_{BL} > 6$ TeV [38]. As we will see in Sec. IV, we fix the value of $M_{Z'} = 4$ TeV, which satisfies all constraints from the LHC and LEP2. Furthermore, LHC constraints from the Drell-Yan (DY) process also exist, which force the $B-L$ Z' mass to be in the few TeV region. This indicates that $m_{\eta_{1,2}}$ and μ' are of order TeV. Therefore, in the scenario of universal soft SUSY breaking terms of the BLSSM, a heavy $M_{Z'}$ implies higher soft terms, hence the estimation of the FT is expected to be worse than in the MSSM. At this point, it is worth mentioning that the Z' gauge boson in the BLSSM can have a large decay width, thus potentially evading LEP and LHC constraints, which are based on the assumption of a narrow decay width, hence on Z' decays into SM particles and additional neutrinos only. While this has been proven to be possible in a nonunified version of the BLSSM, wherein the aforementioned limits can be relaxed and $M_{Z'}$ can be of order one TeV [33,34], it remains to be seen whether a similar phenomenology can occur in the unified version of it which we are going to deal with here.

The paper is organized as follows. In Sec. II, we briefly review the BLSSM with a particular emphasis on the $B-L$ minimization conditions that relate the mass of the neutral gauge boson Z' to the soft SUSY breaking terms and also the extended neutralino sector. Section III is devoted to study the RGEs of the BLSSM matter content as well as the gauge and Yukawa couplings. The collider and DM constraints are addressed in Sec. IV. In Sec. V, we investigate the FT

measures in the BLSSM versus the MSSM case. Section VI presents our numerical results. Finally, our remarks and conclusions are given in Sec. VII.

II. THE $B-L$ SUPERSYMMETRIC STANDARD MODEL

In this section, we briefly review the BLSSM with an emphasis on its salient features with respect to the MSSM. Even though its gauge group seems like a simple extension of the MSSM gauge group with a gauged $U(1)_{B-L}$ (hereafter, $B-L$ symmetry), it significantly enriches the particle content, which drastically changes the low-scale phenomena. First of all, the anomaly cancellation in the BLSSM requires three singlet fields; the most natural candidates in the BLSSM framework are the three right-handed neutrino fields. We may implement the SUSY seesaw mechanisms, where nonzero neutrino masses and mixings consistent with experimental data [39] are achieved. In addition, R-parity, which is assumed in the MSSM to avoid fast proton decay, can be linked to the $U(1)_{B-L}$ gauge group and it can be preserved if the $B-L$ symmetry is broken spontaneously [40], as is the case in the BLSSM studied here.

Spontaneous breaking of the $B-L$ symmetry can be realized in a similar way to the Higgs mechanism. That is, one can introduce two scalar fields, denoted as $\eta_{1,2}$. These fields should carry nonzero $B-L$ charges to break the $B-L$ symmetry and they are preferably singlets under the MSSM gauge group so as not to spoil EWSB. Thus, the superpotential in the BLSSM can be written as

$$W = \mu H_u H_d + Y_u^{ij} Q_i H_u u_j^c + Y_d^{ij} Q_i H_d d_j^c + Y_e^{ij} L_i H_d e_j^c + Y_\nu^{ij} L_i H_u N_i^c + Y_N^{ij} N_i^c N_j^c \eta_1 + \mu' \eta_1 \eta_2, \tag{2.1}$$

where the first line represents the MSSM superpotential using the standard notation for (s)particles while the second line includes the terms associated with the right-handed neutrinos, N_i^cs, plus the singlet Higgs fields η_1 and η_2. The $B-L$ symmetry requires η_1 and η_2 to carry -2 and $+2$ charges under $B-L$ transformations, respectively. The presence of the N_i^c terms makes it possible to have Yukawa interaction terms for the neutrinos, denoted by Y_ν. Finally, μ' stands for the bilinear mixing term between the singlet Higgs fields.

In addition to the right-handed neutrinos and the singlet Higgs fields, the BLSSM also introduces a gauge field (B') and its gaugino ($\tilde{B}'$) associated with the gauged $B-L$ symmetry, so that the appropriate soft SUSY-breaking (SSB) Lagrangian can be written as

$$-\mathcal{L}_{\rm SSB}^{\rm BLSSM} = -\mathcal{L}_{\rm SSB}^{\rm MSSM} + m_{\tilde{N}^c}^2 |\tilde{N}^c|^2 + m_{\eta_1}^2 |\eta_1|^2 + m_{\eta_2}^2 |\eta_2|^2 + A_\nu \tilde{L} H_u \tilde{N}^c + A_N \tilde{N}^c \tilde{N}^c \eta_1 + \frac{1}{2} M_{B'} \tilde{B}' \tilde{B}' + M_{BB'} \tilde{B} \tilde{B}' + B(\mu' \eta_1 \eta_2 + \text{H.c.}). \tag{2.2}$$

Note that, in contrast to its non-SUSY version, the BLSSM does not allow mixing between the doublet and singlet Higgs fields through the superpotential and SSB Lagrangian. Therefore, the scalar potential for these can be written separately and their mass matrices can be diagonalized independently. The scalar potential for the singlet Higgs fields can be derived as

$$V(\eta_1, \eta_2) = \mu_1'^2 |\eta_1|^2 + \mu_2'^2 |\eta_2|^2 - \mu_3' (\eta_1 \eta_2 + \text{H.c.}) + \frac{1}{2} g_{BL}^2 (|\eta_1|^2 - |\eta_2|^2)^2 \tag{2.3}$$

and the minimization of this potential yields Eq. (1.3). Despite the nonmixing superpotential and SSB Lagrangian, one can implement mixing between the two Abelian gauge fields via $-\chi B_{\mu\nu}^{B-L} B^{Y,\mu\nu}$, where $B_{\mu\nu}^a$ is the field strength tensor of a $U(1)$ gauge field, with $a = (Y, B-L)$, the hypercharge and $B-L$ charge, respectively. The gauge kinetic mixing can be rotated away from the kinetic Lagrangian and the covariant derivative takes a noncanonical form [27]

$$D_\mu = \partial_\mu + \cdots + (\tilde{g} Y + g'(B-L)) B'_\mu, \tag{2.4}$$

where $\tilde{g}$ describes the kinetic mixing in place of χ. Even though $\tilde{g}$ is set to zero at the GUT scale, it can be generated at the low scale through the RGEs [41]. In this basis, one finds

$$M_Z^2 \simeq \frac{1}{4}(g_1^2 + g_2^2) v^2, \qquad M_{Z'}^2 \simeq g_{BL}^2 v'^2 + \frac{1}{4} \tilde{g}^2 v^2, \tag{2.5}$$

where $v = \sqrt{v_u^2 + v_d^2} \simeq 246$ GeV and $v' = \sqrt{v_1'^2 + v_2'^2}$ with the vacuum expectation values (VEVs) of the Higgs fields given by $\langle \text{Re} H_{u,d}^0 \rangle = v_{u,d}/\sqrt{2}$ and $\langle \text{Re} \eta_{1,2} \rangle = v'_{1,2}/\sqrt{2}$. It is worth mentioning that the mixing angle between Z and Z' is given by

$$\tan 2\theta' \simeq \frac{2\tilde{g}\sqrt{g_1^2 + g_2^2}}{\tilde{g}^2 + 16(\frac{v'}{v})^2 g_{BL}^2 - g_2^2 - g_1^2}. \tag{2.6}$$

The minimization conditions of the BLSSM scalar potential at tree-level lead to the following relations [27]:

$$v_1' \left(m_{\eta_1}^2 + |\mu'|^2 + \frac{1}{4} \tilde{g} g_{BL} (v_d^2 - v_u^2) + \frac{1}{2} g_{BL}^2 (v_1'^2 - v_2'^2) \right) - v_2' B\mu' = 0, \tag{2.7}$$

$$v_2' \left(m_{\eta_2}^2 + |\mu'|^2 + \frac{1}{4} \tilde{g} g_{BL} (v_u^2 - v_d^2) + \frac{1}{2} g_{BL}^2 (v_2'^2 - v_1'^2) \right) - v_1' B\mu' = 0. \tag{2.8}$$

From these equations, one can determine $|\mu'|^2$ and $B\mu'$ in terms of other soft SUSY breaking terms. (Note that, with $\tilde{g} = 0$, the expression of $|\mu'|^2$ takes the form of Eq. (1.3).)

Breaking the EW and $B-L$ symmetries naturally shapes a type-I seesaw mechanism for the six neutrino states of the model. The effective lepton flavor violating scale is dynamically generated and identified with the $B-L$ one. The resulting 6×6 mass matrix will include these two different breaking scales in two separated 3×3 blocks. The singlet Higgsino VEVs are responsible for the Majorana block in the subspace of right-handed neutrinos whereas EWSB determines the left-right neutrino mixing of a Dirac type. Hierarchies between the two scales, with the Majorana scale much larger than the Dirac one, is the origin of the type-I seesaw mechanism. As a consequence of the additional neutral states $\tilde{B}', \tilde{\eta}_1$ and $\tilde{\eta}_2$, the corresponding neutralino mass matrix is extended to a 7×7 one given by

$$\mathcal{M}_7(\tilde{B},\tilde{W}^3,\tilde{H}_1^0,\tilde{H}_2^0,\tilde{B}',\tilde{\eta}_1,\tilde{\eta}_2)\equiv\begin{pmatrix}\mathcal{M}_4 & \mathcal{O}\\ \mathcal{O}^T & \mathcal{M}_3\end{pmatrix}, \tag{2.9}$$

where $\mathcal{M}_4$ is the MSSM-type neutralino mass matrix and $\mathcal{M}_3$ is the additional 3×3 neutralino mass matrix, which is given by

$$\mathcal{M}_3=\begin{pmatrix}M_{B'} & -g_{BL}v_1' & g_{BL}v_2'\\ -g_{BL}v_1' & 0 & -\mu'\\ g_{BL}v_2' & -\mu' & 0\end{pmatrix}. \tag{2.10}$$

In addition, the off-diagonal matrix $\mathcal{O}$ is given by

$$\mathcal{O}=\begin{pmatrix}M_{BB'} & 0 & 0\\ 0 & 0 & 0\\ -\frac{1}{2}\tilde{g}v_d & 0 & 0\\ \frac{1}{2}\tilde{g}v_u & 0 & 0\end{pmatrix}. \tag{2.11}$$

(Note that the off-diagonal matrix elements vanish identically if $\tilde{g}=0$ and $M_{BB'}=0$). One can then diagonalize the real matrix $\mathcal{M}_7$ with a symmetric mixing matrix V such that

$$V\mathcal{M}_7V^T=\mathrm{diag}(m_{\tilde{\chi}_k^0}),\qquad k=1,\ldots,7. \tag{2.12}$$

In these conditions, the LSP has the following decomposition:

$$\begin{aligned}\tilde{\chi}_1^0=&V_{11}\tilde{B}+V_{12}\tilde{W}^3+V_{13}\tilde{H}_d^0+V_{14}\tilde{H}_u^0+V_{15}\tilde{B}'\\&+V_{16}\tilde{\eta}_1+V_{17}\tilde{\eta}_2.\end{aligned} \tag{2.13}$$

If the LSP is then considered as a candidate for DM, each species in the above equation, if dominant, leads to its own phenomenology that can possibly be distinguished in direct detection experiments. For example, to achieve the correct relic density of binolike DM is challenging, since its abundance is usually so high over the fundamental parameter space that one needs to identify several annihilation and/or coannihilation channels to reduce its density down to the WMAP [6] or Planck [7] measurements. Since this DM state interacts through the hypercharge, its scattering with nuclei has a very low cross section. Conversely, the largest cross section in DM scattering can be obtained when DM is Higgsino-like, since it interacts with the quarks through the Yukawa interactions. Since the BLSSM sector offers significant interference in the neutralino sector, this may also drastically change the DM kinematics. In contrast to a bino, the $\tilde{B}'$-ino interacts more strongly depending on the $B-L$ gauge coupling. Despite the severe mass bound on the Z', there is no specific bound on $m_{\tilde{B}'}$, so that it can be even as low as 100 GeV [42]. In this context, one can expect the LSP neutralino to be mostly formed by $\tilde{B}'$ and its cross section in its scattering with nuclei can be very large, in contrast to the bino case. In addition to $\tilde{B}'$, the LSP neutralino can be formed by the singlet Higgsinos (also dubbed bileptinos due to their $L=\pm 2$ lepton charge). In this case, it is challenging for their abundance to be compatible with the experimental results. The reduction through the coannihilation channels involving SUSY particles arises from the gauge kinetic mixing, which is restricted to be moderate. If its mass is nearly degenerate with that of the $\tilde{B}'$ state, they can significantly coannihilate. Also, a singlet Higgsino yields low cross section in DM scattering experiments. Besides the neutralinos, one can also consider the sneutrino as a DM candidate, when it is the LSP. In this case, the extended sector of the BLSSM involves twelve states coming from the superpartners of the left- and the right-handed neutrinos. In a Charge and Parity (CP)-conserving framework the states entering the sneutrino mixing matrix can be expressed by separating their scalar and pseudoscalar components:

$$\tilde{\nu}_i=\frac{\sigma_{Li}+i\phi_{Li}}{\sqrt{2}},\qquad \tilde{N}_i=\frac{\sigma_{Ri}+i\phi_{Ri}}{\sqrt{2}}. \tag{2.14}$$

The breaking of $B-L$ generates an effective mass term through $Y_N^{ij}N_i^cN_j^c\eta_1$ causing a mass splitting between the CP-even and CP-odd sector. Therefore, in terms of Eq. (2.14), the corresponding 12×12 mass matrix is reduced to two different 6×6 blocks

$$\begin{aligned}\mathcal{M}^{2\sigma}(\sigma_L,\sigma_R)&\equiv\begin{pmatrix}\mathcal{M}_{LL}^{2\sigma} & \mathcal{M}_{LR}^{2\sigma}\\ \mathcal{M}_{LR}^{2\sigma\ T} & \mathcal{M}_{RR}^{2\sigma}\end{pmatrix},\\ \mathcal{M}^{2\phi}(\phi_L,\phi_R)&\equiv\begin{pmatrix}\mathcal{M}_{LL}^{2\phi} & \mathcal{M}_{LR}^{2\phi}\\ \mathcal{M}_{LR}^{2\phi\ T} & \mathcal{M}_{RR}^{2\phi}\end{pmatrix}.\end{aligned} \tag{2.15}$$

Such differences between CP-even and CP-odd sectors do not involve the left components with $\mathcal{M}_{LL}^{\sigma}$ and $\mathcal{M}_{LL}^{\phi}$ described by the common form $\mathcal{M}_{LL}^2$

$$\mathcal{M}_{LL}^{2\,i,j} \equiv \frac{\delta^{i,j}}{8}((g_1^2+g_2^2+\tilde{g}(g_{BL}+\tilde{g}))\delta_H + (g_{BL}+\tilde{g})\delta_\eta) + \frac{1}{2}v_u^2(Y_\nu^T Y_\nu)^{i,j} + m_l^{2\,i,j}, \tag{2.16}$$

where we have introduced $\delta_\eta = v_1'^2 - v_2'^2$ and $\delta_H = v_d^2 - v_u^2$. For the submatrices $\mathcal{M}_{RR}^{2\sigma}$ and $\mathcal{M}_{RR}^{2\phi}$, we have instead

$$\mathcal{M}_{RR}^{2\,i,j} \equiv -\frac{\delta^{i,j}}{8}g_{BL}(\tilde{g}\delta_H + 2g_{BL}\delta_\eta) + \frac{1}{2}v_u^2(Y_\nu Y_\nu^T)^{i,j} + m_{\tilde{N}}^{2\,i,j} + 2v_1'^2(Y_N^2)^{i,j} \mp \sqrt{2}(v_2'\mu' Y_N^{i,j} - v_1' A_N^{i,j}) \tag{2.17}$$

while the left-right sneutrino mixing is ruled by the matrices

$$\mathcal{M}_{LR}^{2\,i,j} \equiv \frac{1}{2}(-\sqrt{2}v_d\mu Y_\nu^{i,j} + v_u\sqrt{2}A_\nu^{i,j} \pm 2v_u v_1'(Y_N Y_\nu)^{i,j}), \tag{2.18}$$

with upper (lower) signs corresponding to CP-even (odd) cases. The parameter Y_ν and the corresponding trilinear term A_ν determine the mixing between the left and right components. In our setup, Y_ν is negligible and can safely be set to zero already at the GUT scale, as it is the case also for the boundary condition of A_ν. The resulting 12×12 sneutrino mass matrix is consequently unable to mix the left- and right-handed components as the CP-even and CP-odd parts of a sneutrino state will be completely determined by assigning its CP value and the chirality of its supersymmetric partner.

III. RENORMALIZATION GROUP EQUATIONS

The presence of an extra Abelian gauge group introduces a distinctive feature, the gauge kinetic mixing, through a renormalizable and gauge invariant operator $\chi B^{\mu\nu}B'_{\mu\nu}$ of the two Abelian field strengths. Moreover, off-diagonal soft breaking terms for the Abelian gaugino masses are also allowed. This effect is completely novel with respect to the MSSM or other supersymmetric models in which only a single $U(1)$ factor is considered. If the two Abelian gauge factors emerge from the breaking of a simple gauge group, the kinetic mixing is absent at that scale. For this reason, arguing that the BLSSM could be embedded into a wider GUT scenario (the matter content of the BLSSM, which includes three generations of right-handed neutrinos, nicely fits into the 16-D spinorial representation of $SO(10)$), we require the vanishing of the kinetic mixing at the GUT scale. As we stated above, we nevertheless end up with a nonzero kinetic mixing at low scales affecting the Z' interactions as well as the Higgs and the neutralino sectors [27].

Instead of working with a noncanonical kinetic Lagrangian in which the kinetic mixing χ appears, it is more practical to introduce a nondiagonal gauge covariant derivative with a diagonal kinetic Lagrangian. The two approaches are related by a gauge field redefinition and are completely equivalent. In this basis the covariant derivative of the Abelian fields takes the form $\mathcal{D}_\mu = \partial_\mu - iQ^T G A_\mu$, where Q is the vector of the Abelian charges, A is the vector of the Abelian gauge fields and G is the Abelian gauge coupling matrix with nonzero off-diagonal elements. The matrix G can be recast into a triangular form with an orthogonal transformation $G \to GO^T$ [43]. With this parametrization, the three independent parameters of G are explicitly manifest and correspond to the Abelian couplings, g_1, g_{BL} and $\tilde{g}$, describing, respectively, the hypercharge interactions, the extra $B-L$ ones and the gauge kinetic mixing. Differently from the MSSM case, the Abelian gaugino mass term is replaced by a symmetric matrix with a nonzero mixed mass term $M_{BB'}$ between the B and B' gauginos. Coherently with our high-energy unified embedding, we choose $M_{BB'} = 0$ at the GUT scale. Notice that the Abelian gaugino mass matrix M is affected by the same rotation O and in the basis in which G is triangular and M transforms through $M \to OMO^T$.

We have performed an RGE study of the BLSSM assuming gauge coupling unification and minimal supergravity (mSUGRA) boundary conditions at the GUT scale. This scenario considerably constrains the parameter space connecting different sectors which are usually independent in nonunified scenarios. In particular, the two main scales describing BSM physics, the scale of SUSY and $B-L$ breaking, are linked by the RGEs. In a non-SUSY model, the $B-L$ symmetry breaking scale is arbitrary and can be placed anywhere between TeV and GUT energies. However, within a SUSY scenario, the radiative symmetry breaking approach can also be applied to $B-L$ symmetry breaking. This mechanism was studied for the first time in [20]. As discussed in detail herein, radiative $B-L$ symmetry breaking requires $m_{\eta_1} \neq m_{\eta_2}$ at the low scale. This requirement relates then the $B-L$ symmetry breaking scale to the SUSY one, since $m_{\eta_{1,2}}$ are SSB masses for the relevant Higgs fields denoted by η_i.

The two-loop RGEs have been computed with SARAH [44] and fed into SPheno [45] which has been used for the spectrum computation and for the numerical analysis of the model. Here we show the one-loop β functions of the gauge couplings highlighting the appearance of the kinetic mixing contributions,

$$\begin{aligned}
\beta_{g_1}^{(1)} &= \frac{33}{5}g_1^3,\\
\beta_{g_{BL}}^{(1)} &= \frac{3}{5}g_{BL}(15g_{BL}^2 + 4\sqrt{10}g_{BL}\tilde{g} + 11\tilde{g}^2),\\
\beta_{\tilde{g}}^{(1)} &= \frac{3}{5}\tilde{g}(15g_{BL}^2 + 4\sqrt{10}g_{BL}\tilde{g} + 11\tilde{g}^2) + \frac{12\sqrt{10}}{5}g_1^2 g_{BL},\\
\beta_{g_2}^{(1)} &= g_2^3,\\
\beta_{g_3}^{(1)} &= -3g_3^3,
\end{aligned} \tag{3.1}$$

where we have adopted the GUT normalizations $\sqrt{3/5}$ and $\sqrt{3/2}$, respectively, for the $U(1)_Y$ and $U(1)_{B-L}$ gauge groups. At one-loop level the expressions of the β functions of g_1, g_2 and g_3 are the same as those of the MSSM with differences appearing at two-loop order only. Notice that the term responsible for the reintroduction of a nonvanishing mixing coupling $\tilde{g}$ along the RGE running, even if absent at some given scale, is the last term in $\beta_{\tilde{g}}^{(1)}$. We recall again that the kinetic mixing is a peculiar feature of Abelian extensions of the SM and their supersymmetric versions, admissible only between two or more $U(1)$ gauge groups.

Assuming gauge coupling unification at the GUT scale, the RGE analysis provides the results $\tilde{g} \simeq -0.144$ and $g_{BL} \simeq 0.55$ with $M_{\rm GUT} \simeq 10^{16}$ GeV, which are controlled by the leading one-loop β functions given in Eq. (3.1). The spread of points around these central values, less than 1% for g_{BL} and 5% for $\tilde{g}$, is only due to higher-order corrections, namely two-loop running and threshold corrections.

The running of the gaugino masses is directly linked to that of the gauge couplings. In the Abelian sector and at one loop, the Abelian gaugino mass matrix M evolves with

$$\beta_M = MG^T Q^2 G + G^T Q^2 GM = MG^{-1}\beta_G + G^{-1}\beta_G M, \tag{3.2}$$

where $Q = \sum_p Q_p Q_p^T$, with Q_p the vector of the Abelian charges of the p particle. Exploiting the structure of the β functions of the gaugino masses, a simple relation is obtained, $M_i/m_{1/2} = g_i^2/g_{\rm GUT}^2$, for non-Abelian masses at one-loop order. In the Abelian sector, due to the presence of the mixing, the previous equation is replaced by a matrix relation. Indeed, from the product $GM^{-1}G^T$, which remains constant along the RGE evolution, one finds the Abelian gaugino mass matrix $M/m_{1/2} = G^T G/g_{\rm GUT}^2$. We show in Fig. 1 the dependence of the gaugino masses as a function of the GUT gaugino mass $m_{1/2}$. The hierarchy is obviously controlled by the size of the gauge couplings at low scale.

The gaugino masses M_1, M_1' and $\tilde{M}$ are obtained from M_B, $M_{B'}$ and $M_{BB'}$ through the transformation OMO^T. The coefficients $\sigma_{1,2}$ are defined as

$$\begin{aligned}\sigma_1 &= m_{H_d}^2 - m_{H_u}^2 - \mathrm{tr}(m_d^2) - \mathrm{tr}(m_e^2) + \mathrm{tr}(m_l^2) \\ &\quad - \mathrm{tr}(m_q^2) + 2\mathrm{tr}(m_u^2), \\ \sigma_2 &= 2m_{\eta_1}^2 - 2m_{\eta_2}^2 + \mathrm{tr}(m_d^2) - \mathrm{tr}(m_e^2) \\ &\quad + 2\mathrm{tr}(m_l^2) - 2\mathrm{tr}(m_q^2) + \mathrm{tr}(m_u^2) - \mathrm{tr}(m_{\nu_R}^2)\end{aligned} \tag{3.3}$$

and are found to be RGE invariant combinations of the soft SUSY masses. Assuming unification conditions at the GUT scale, $\sigma_{1,2}$ remain zero along all the RGE evolution. As $\beta_{m_{\eta_2}^2}$ is only characterized by negative contributions proportional to the Abelian gaugino masses, the corresponding soft mass $m_{\eta_2}^2$ will increase and remain positive during the run from the GUT to the EW scale. The same feature is shared by $m_{H_d}^2$ except for some particular values of the gaugino and soft scalar masses at the GUT scale for which the Y_b Yukawa coupling contribution (of the b-quark) to $\beta_{m_{\eta_2}^2}$ is not negligible. The spontaneous symmetry breaking of EW and B-L, requiring negative $m_{H_u}^2$ and $m_{\eta_1}^2$, can be realized radiatively, which is a nice feature in both MSSM and BLSSM. Namely, even though there is no spontaneous symmetry breaking at a high scale, the large top-quark Yukawa coupling Y_t and its trilinear soft term A_t can drive $m_{H_u}^2$ negative through its RGE evolution, which triggers spontaneous EWSB. Similarly, a sufficiently large neutrino Yukawa coupling Y_N and corresponding trilinear soft term A_n turn $m_{\eta_1}^2$ negative in its RGE evolution and break the $B-L$ symmetry spontaneously.

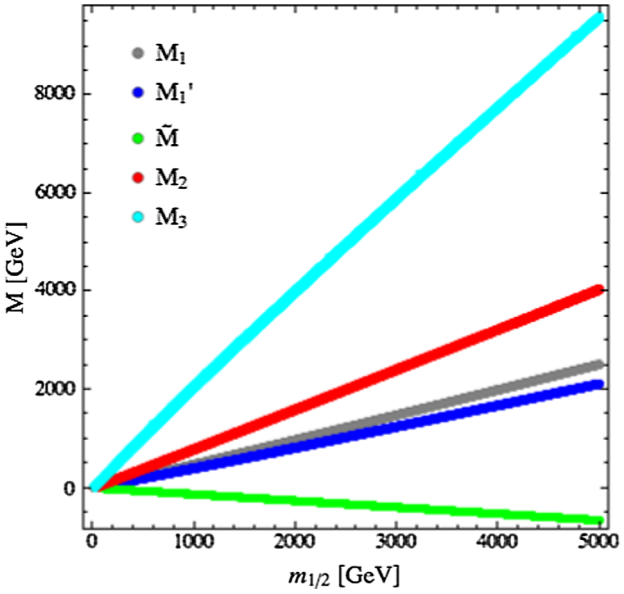

FIG. 1. Gaugino masses at the SUSY scale as a function of the GUT $m_{1/2}$ mass. Here, both gauge coupling and soft mass unification have been assumed.

In general only one of the three components of the diagonal Y_N matrix is required to be large in order to realize the spontaneous symmetry breaking of the extra Abelian symmetry, thus providing a heavy and two possible lighter heavy-neutrino states. Notice also that the elements of the low-scale values of the Y_N matrix cannot be taken arbitrary large otherwise a Landau pole is hit before the GUT scale. A close inspection of the one-loop β function of the heavy-neutrino Yukawa coupling

$$\beta_{Y_N} = 8Y_N Y_N^* Y_N + 2\mathrm{tr}(Y_N Y_N^*)Y_N - \frac{9}{2}{g_{BL}}^2 Y_N, \tag{3.4}$$

where we have neglected the negligible contribution of the light-neutrino Yukawa coupling Y_ν, shows that $Y_N \gtrsim 0.5$

spoils indeed the perturbativity of the model at the GUT scale or below.

IV. COLLIDER AND DARK MATTER CONSTRAINTS

To investigate the viability of the BLSSM parameter space, with mSUGRA boundary conditions, we have challenged its potential signatures against two sets of experimental constraints. To the first set belong different bounds coming from collider probes which have been used in building the scan procedure. These form a varied set of requirements affecting our choice of the Z' benchmark mass as well as the character of the acceptable low-scale particle spectrum. As already stated, stringent constraints come from LEP2 data via EW precision observables (EWPOs) and from run 2 of the LHC through a signal-to-background analysis using Poisson statistics to extract a 95% confidence level (C.L.) bound in the di-lepton channel. The C.L. has been extracted at the LHC with $\sqrt{s} = 13$ TeV and $\mathcal{L} = 13.3$ fb^{-1}, updating the analysis presented in [46]. We have taken into account the Z' signal and its interference with the SM background and included efficiency and acceptance for both the electron and muon channels as described in [47]. Such studies affect the extended gauge sector $(\tilde{g}, g_{BL}, M_{Z'})$ in a way that, in all safety, allow us to select the value $M_{Z'} = 4$ TeV for all magnitudes of gauge couplings and Z' total width (in the range 30–45 GeV) met in the RGE evolution. Notice that the BLSSM supplied with unification conditions at the GUT scale provides a very narrow Z' width with a $\Gamma_{Z'}/M_{Z'}$ ratio reaching 1% at most. Thus, this is unlike the results of [33,34], which were indeed obtained without any universality conditions. Such a Z' mass value completes the independent parameters that feed our scan and which in turn provides a BLSSM low-energy spectrum. We now impose the exclusion bounds coming from LEP, Tevatron and LHC linked to the negative searches of scalar degrees of freedom and to the correct reproduction of the measured Higgs signal strength around 125 GeV. More precisely, from our scan it is possible to extract the masses and the branching ratios (BRs) of all the (neutral and charged) scalars plus their effective couplings to SM fermions and bosons. This information is then processed into HiggsBounds [48–51] which, considering all the available collider searches, expresses whether a parameter point has been excluded at 95% C.L. or not.

This analysis removes a considerable number of acceptable points, among those with successful EW and $U(1)_{B-L}$ symmetry breaking, as obtained from the GUT parameters scan. Over such points, the compatibility fit of the generated Higgs signal strengths with the ones measured at LHC is taken into account by HiggsSignals [52], which provides the corresponding χ^2. By asking for a 2σ interval around the minimum χ^2 generated, we obtain a further constraint over the parameter space investigated. The strongest sparticle bounds which may affect our generated SUSY spectra come from the mass limits on the chargino and stau sectors, which must be more massive than $\approx$100 GeV [53]. However, for our generated sparticles, we are safe from this limit.

The second set of bounds that we considered emerges from the probe of DM signatures which are a common and natural product of many SUSY models. Among these, the BLSSM stands out for both theoretical and phenomenological reasons that make the study of its DM aspects particularly worthwhile. The presence of a gauged $B-L$ symmetry, being broken by the scalar fields η_1 and η_2, as they are charged under $B-L$ [21], provides a local origin to the discrete R symmetry that is usually imposed *ad hoc* to prevent fast proton decay. Consequently, the BLSSM embeds the stability of the LSP through its gauge structure, as it does for the produced DM density.

From the phenomenological side, the BLSSM, like the MSSM, has the neutralino as a possible cold DM candidate. The presence of additional neutral degrees of freedom drastically changes its properties with respect to the corresponding MSSM ones, which is mostly bino in GUT constrained models, possibly giving the necessary degrees of freedom to accommodate the measured DM evidences. Moreover, the BLSSM also envisages a scalar LSP in its spectrum, generated by the superpartners of the six Majorana neutrinos, which may also be the origin of a cold DM relic.

For every possible low-energy spectrum obtained, the LSP provided by the BLSSM will participate in the early thermodynamical evolution of the universe. After an initial regime of thermal equilibrium with the SM particles, decoupling takes place once the DM annihilation rate becomes slower than the Universe expansion. This process would result in the relic density lasting until now. Consequently, a crucial test of the cosmological viability of the BLSSM is enforced by requiring the relic abundance generated not to overclose the Universe by exceeding the measured current value of the DM relic density,

$$\Omega h^2 = 0.1187 \pm 0.0017(\text{stat}) \pm 0.0120(\text{syst}), \qquad (4.1)$$

as measured by the Planck Collaboration [7].

The requirement to reproduce the measured relic density would finally highlight the region of the parameter space where the model is able to solve the DM puzzle. The computation of the DM abundance is achieved by solving the evolution numerically with MicrOMEGAs [54,55], which collects the amplitudes for all the annihilation, as well as coannihilation, processes. Another source of constraints, which cannot be neglected due to the recent increase in precision reached by the LUX Collaboration [4,56], is linked to the direct searches intended to detect DM signatures coming from DM scatterings with nuclei. We have tested the BLSSM spectrum against the challenging upper limit on the

spin independent (SI) component of the LSP-nucleus scattering. The zeptobarn order of magnitude, reached in the recent upgrade of the DM-nucleus cross section bound, will have an interesting interplay with the parameter space analyzed to test the surviving ability of the BLSSM against stringent exclusions.

The DM scenarios provided represent a peculiar signature of the model, with characteristic degrees of freedom playing a key role in drawing a rich DM texture. As already stated, the BLSSM has two candidates for cold DM as it is possible to have, other than the neutralino, also a heavy stable sneutrino. The extended neutral sector, consequence of the inclusion of an extra $B-L$ gauge factor, enlarges the neutralino components with three new states (two coming from bileptinos and one from BLino) as seen in Eq. (2.13). To study the behavior of the neutralinos we may consider the following classification:

$V_{11}^2 > 0.5$	Binolike,
$V_{12}^2 > 0.5$	Winolike,
$V_{13}^2 + V_{14}^2 > 0.5$	Higgsino-like,
$V_{15}^2 > 0.5$	BLino-like,
$V_{16}^2 + V_{17}^2 > 0.5$	Bileptinolike,
Neither of the previous cases	Mixed.

In this scheme, the nature of the neutralino is identified with the interaction eigenstate that makes up for more than half of its content.

For all the points generated in our scan, in agreement with the constraints from Higgs searches, the LSP will, in the majority of cases, results in a fermionic DM candidate with mass below 2 TeV; see Fig. 2(a). The sneutrino will instead be a subdominant option over our entire set of points. It is interesting to explore the composition of the sneutrino LSP written in terms of *CP* eigenstates and left-right parts. This is relevant to appreciate the chances to survive the direct detection probes of DM, with a left-handed sneutrino having a dangerously enhanced scattering rate against nuclei [57] due to Z mediation. Figure 3 indicates that only sneutrinos above ∼2 TeV may have a large left handed component. However, we will see only sneutrinos lighter than this limit will compete against the neutralino as a possible LSP. So, the LSP sneutrino in our constrained BLSSM will always be a *right*-handed sneutrino. Following the previous classification, a binolike neutralino will be more common to encounter as the BLSSM favorite LSP, but, as typical features of the model, also states of BLino and bileptino nature are often met; see Fig. 2(b). Notably, no Higgsino-like neutralino are found while the wino possibility is a most rare one, which requires very tuned conditions over the parameter space to be produced in a sizeable amount. Given our uniform treatment over the boundary conditions, we will not consider this case though.

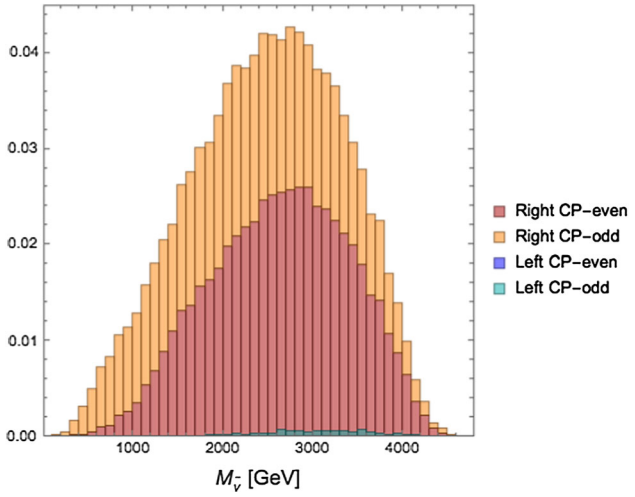

FIG. 3. Composition of the lightest sneutrino for the set of points in agreement with the constraints from HiggsBounds and HiggsSignals. Histogram is of stacked type with normalized heights.

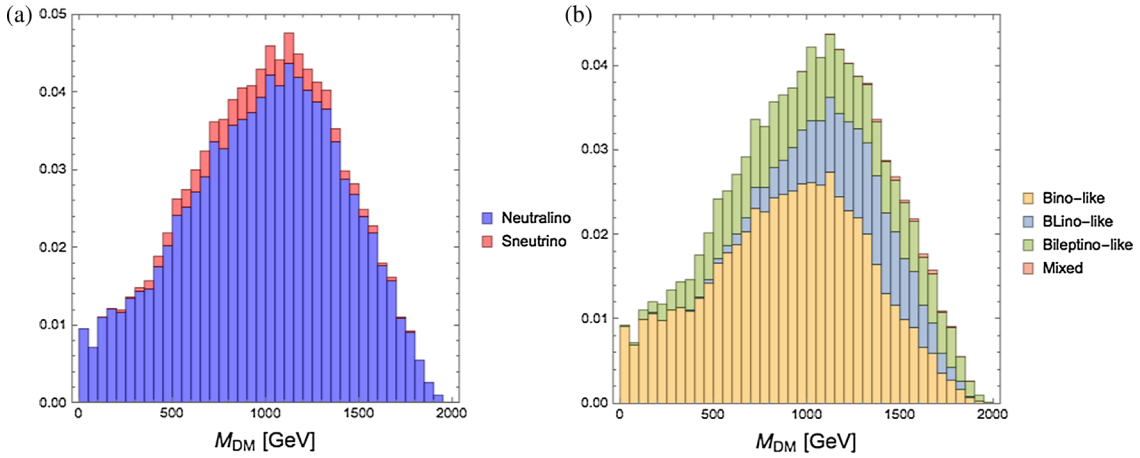

FIG. 2. (a) The normalized distribution of the neutralino and sneutrino types found in our scan. (b) The normalized distribution of the different types of LSP found in our scan. The histograms are stacked.

V. FINE-TUNING MEASURES

We introduce measures of FT in this section to compare BLSSM and MSSM in respect of naturalness. FT is not a physical observable, but it is rather an indication for an unknown mechanism, which is missing in the model under concern. Its quantitative values, then, can be interpreted as the effectiveness of the missing mechanisms over the low-scale results. In this context, the model may cover most of the whole BSM physics, when FT is small.

There are many alternatives for a quantitative measure of FT [37,58–71], which are commonly based on the change in the Z-boson mass. Its measure (denoted by Δ) equals the largest of these changes defined as [72,73]

$$\Delta = \mathrm{Max}\left|\frac{\partial \ln v^2}{\partial \ln a_i}\right| = \mathrm{Max}\left|\frac{a_i}{v^2}\frac{\partial v^2}{\partial a_i}\right| = \mathrm{Max}\left|\frac{a_i}{M_Z^2}\frac{\partial M_Z^2}{\partial a_i}\right|. \tag{5.1}$$

When viewing a parameter space, a particular point has a low FT if the Z mass does not largely change when deviating from its position. A natural model will, therefore, possess large regions of viable parameter space with low FT values. Having this feature in a particular model will make it more attractive a prospect. Our goal here is to find allowed regions of parameter space for the BLSSM with a similar (or better) level of FT to the MSSM, so the models may be of comparable naturalness. In this paper, we apply this same measure in two different scenarios (high- and low-scale parameters) for both the MSSM and BLSSM. We will proceed by explaining the procedure for the two models. We compute the minimization conditions, or tadpole equations, and solve them to find a relation for the Z-mass and SUSY-scale parameters. At this point, we have two choices: to use these SUSY-scale parameters or to relate these to high-scale (GUT) ones and use those. For the GUT-FT, we treat loop corrections as dependent on the EW VEV, as done in [74], which will eventually reduce the FT value by up to a factor of ~ 2. For the SUSY-FT case, we use the approximation that loop factors are independent of the other parameters, e.g., the Higgs masses (m_{H_u} and m_{H_d}). Notice, in fact, that this approximation has been widely used in the literature [3,71,75–82], hence we have adopted it here too. However, what is important in this work is not the comparison of the two FT methods, but rather for each one of these the difference between the two SUSY models at hand. With this in mind, we begin first by discussing the high- and low-scale scenarios for the MSSM, and proceed to extend this discussion to the BLSSM.

For the GUT-FT in the MSSM, our high-scale parameters are the unification masses for scalars (m_0) and gauginos ($m_{1/2}$), the universal trilinear coupling (A_0), the μ parameter and the quadratic soft SUSY term ($B\mu$),

$$a_i = \{m_0, m_{1/2}, A_0, \mu, B\mu\}. \tag{5.2}$$

In order to calculate this FT measure for a particular spectrum point, the high-scale parameters are altered slightly and a new SUSY spectrum is calculated using the two-loop RGEs to run from GUT to SUSY scale. These new (modified) SUSY-scale parameters (eg m_{H_d}) are used to solve the tadpole equations and calculate a new M_Z. Practically, this computation is implemented in the `SPheno` program [45] and performed automatically for each spectrum point.

The GUT-FT will compare the naturalness at high scale, but two models with similar measures here may have large differences at the SUSY-scale. To test whether the BLSSM and MSSM have a similar FT at both GUT and SUSY-scale, we will consider a low-scale FT. To do this, we begin with the relation for the Z-mass and SUSY-scale parameters,

$$\frac{1}{2}M_Z^2 = \frac{(m_{H_d}^2 + \Sigma_d) - (m_{H_u}^2 + \Sigma_u)\tan^2\beta}{\tan^2\beta - 1} - \mu^2, \tag{5.3}$$

where

$$\Sigma_{u,d} = \frac{\partial \Delta V}{\partial v_{u,d}^2}. \tag{5.4}$$

Unlike in the GUT-FT case, we treat the loop corrections as independent of the EW VEV, as in [71]. If we substitute this expression into Eq. (5.1) and use the low-scale parameters $a_i = \{m_{H_d}^2, m_{H_u}^2, \mu^2, \Sigma_u, \Sigma_d\}$, one will find [71]

$$\Delta_{\mathrm{SUSY}} \equiv \mathrm{Max}(C_i)/(M_Z^2/2), \tag{5.5}$$

where

$$C_i = \begin{cases} C_{H_u} = \left|m_{H_u}^2 \dfrac{\tan^2\beta}{(\tan^2\beta - 1)}\right|, & C_{H_d} = \left|m_{H_d}^2 \dfrac{1}{(\tan^2\beta - 1)}\right|, \\ C_\mu = |\mu^2|, & C_{\Sigma_u} = \left|\Sigma_u \dfrac{\tan^2\beta}{(\tan^2\beta - 1)}\right|, \quad C_{\Sigma_d} = \left|\Sigma_d \dfrac{1}{(\tan^2\beta - 1)}\right|. \end{cases} \tag{5.6}$$

We now turn to the BLSSM. For the GUT-FT, we follow the same universal parameters as the MSSM, but with two additional terms, relating to the μ' parameter and the corresponding quadratic soft SUSY term, $B\mu'$, so that all of our high-scale terms are

$$a_i = \{m_0, m_{1/2}, A_0, \mu, B\mu, \mu', B\mu'\}. \tag{5.7}$$

We may also follow our previous procedure to find a SUSY-scale FT (SUSY-FT) for the BLSSM. By minimizing the scalar potential, we find (at loop level),

$$\frac{Mz^2}{2} = \frac{1}{X}\left(\frac{m_{H_d}^2 + \Sigma_d}{(\tan^2(\beta)-1)} - \frac{(m_{H_u}^2 + \Sigma_u)\tan^2(\beta)}{(\tan^2(\beta)-1)} + \frac{\tilde{g}M_{Z'}^2 Y}{4g_{BL}} - \mu^2\right), \tag{5.8}$$

where

$$X = 1 + \frac{\tilde{g}^2}{(g_1^2+g_2^2)} + \frac{\tilde{g}^3 Y}{2g_{BL}(g_1^2+g_2^2)}, \tag{5.9}$$

and

$$Y = \frac{\cos(2\beta')}{\cos(2\beta)} = \frac{(\tan^2\beta+1)(1-\tan^2\beta')}{(1-\tan^2\beta)(\tan^2\beta'+1)}. \tag{5.10}$$

In the limit of no gauge kinetic mixing ($\tilde{g} \to 0$), this equation reproduces the MSSM minimized potential of Eq. (5.3). Our SUSY-FT parameters for the BLSSM are thus

$$C_i = \begin{cases} C_{H_u} = \left|\frac{m_{H_u}^2}{X}\frac{\tan^2\beta}{(\tan^2\beta-1)}\right|, & C_{H_d} = \left|\frac{m_{H_d}^2}{X}\frac{1}{(\tan^2\beta-1)}\right|, \quad C_{\Sigma_d} = \left|\frac{\Sigma_d}{X}\frac{1}{(\tan^2\beta-1)}\right| \\ C_{\Sigma_u} = \left|\frac{\Sigma_u}{X}\frac{\tan^2\beta}{(\tan^2\beta-1)}\right|, & C_\mu = \left|\frac{\mu^2}{X}\right|, \quad C_{Z'} = \left|M_{Z'}^2\frac{\tilde{g}Y}{4g_{BL}X}\right|. \end{cases} \tag{5.11}$$

These equations resemble those of the MSSM SUSY-FT, but now with a factor of $1/X$. In addition, we have a contribution from the Z' mass and BLSSM loop factors. Considering the heavy mass bound on $M_{Z'}$, its contribution could be expected much larger than the other terms in Eq. (5.8), which would worsen the required FT at the low scale. However, a significantly large $M_{Z'}$ severely constrains the VEVs of the singlet Higgs fields as $\tan\beta' \sim 1$ [27] and, hence, Y yields a very stringent suppression in $C_{Z'}$. Note that, even though the trilinear A-terms are not included in determining the FT, their effects can be counted in the SSB masses in Eq. (5.11), whose values include also the loop corrections.

If the required FT measure is quantified in terms of the GUT scale parameters, as done for the MSSM in [72], such as m_0, $m_{1/2}, A_0, \mu, B\mu, \mu', B\mu'$, one can investigate which parameter is most frequently responsible for determining FT. Since the value of FT is taken to be equal to the maximum contribution out of all parameters, for a given SUSY spectrum only one parameter will determine the FT.

Figure 4 displays the FT contributions of the fundamental parameters of the MSSM and BLSSM. For each of our SUSY spectrum points which survive the HiggsBounds / HiggsSignals constraints, we count the number of times each parameter determines the FT. This has been done for both MSSM and BLSSM points, then the vertical axis is rescaled so the sum of counts is 1.

The dominating term in both cases is from the μ term, which is fixed (along with $B\mu$) by requiring EWSB. The next largest contribution to the FT measure arises from the gaugino sector, whose masses are parametrized via $m_{1/2}$. This can be understood with the heavy gluino mass bound

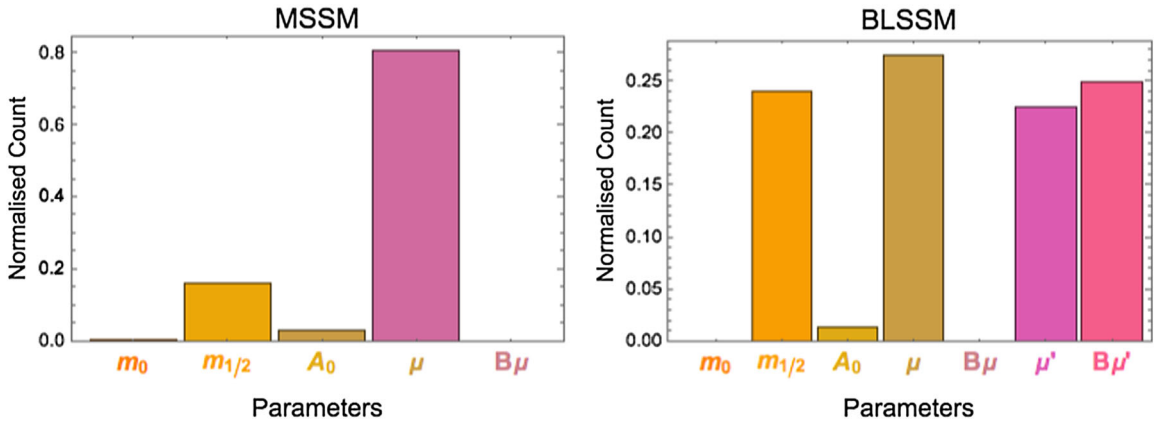

FIG. 4. Histogram for GUT-FT parameters for MSSM (left) and BLSSM (right), counting the number of spectrum points each parameter determines the FT value, and normalized so the sum of counts is unity.

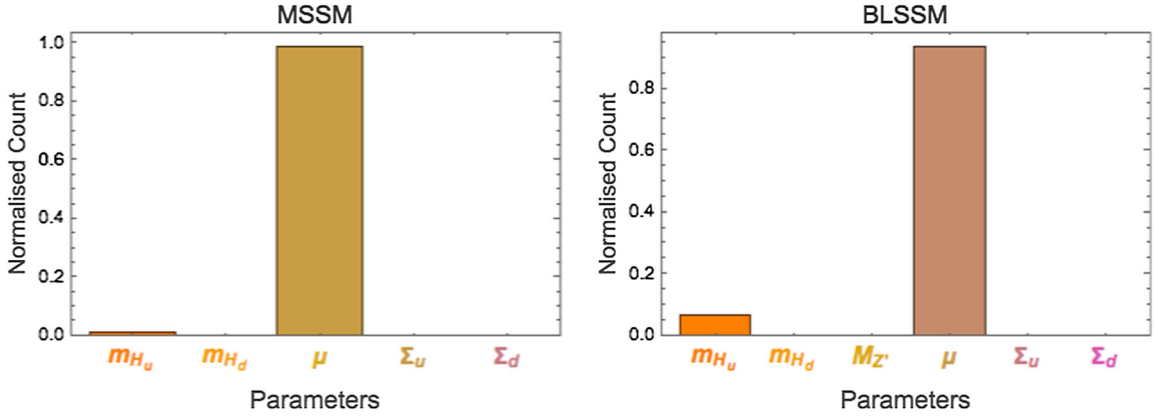

FIG. 5. Histogram for SUSY-FT parameters for MSSM (left) and BLSSM (right), counting the number of spectrum points each parameter determines the FT value, and normalized so the sum of counts is unity.

[83] and its large loop contribution to realize the 125 GeV Higgs boson. The BLSSM sector is also effective in the FT in terms of μ' and $B\mu'$. There is a very small dependence on A_0 as discussed previously, and approximately no dependence on m_0 or $B\mu$ in either case.

Figure 5 uses the same method as Fig. 4, counting the frequency each parameter determines the FT, but now for SUSY-scale parameters. Both the MSSM and BLSSM are dominated by the μ's FT, with a small contribution from m_{H_u} and also a slight dependence on $M_{Z'}$ for the BLSSM. Considering this, what will affect the FT between the BLSSM and MSSM will be a combination of how large the factor X is and the largeness of μ in both models. This value will not be identical, as there is an additional factor of $\frac{M_{Z'}(\tilde{g}Y)}{4g_{BL}}$ in the BLSSM minimization equation.

VI. RESULTS

We will now compare the FT obtained in the BLSSM and MSSM scenarios, for our two FT measures. We will begin by explaining the interval ranges of our data, then we will discuss the SUSY-scale and GUT-scale FTs and which parameters are most responsible for their values. This will be done for both the BLSSM and MSSM, though the same parameters in both models are usually responsible for the largeness of FT. Then we will compare the GUT-FT and SUSY-FT for both the BLSSM and MSSM in the plane $(m_0, m_{1/2})$, as is commonly done.

The scan performed to obtain this data has been done by SPheno with all points being passed through HiggsBounds and HiggsSignals. We have scanned over the range [0, 5] TeV in both m_0 and $m_{1/2}$, $\tan\beta$ in [0, 60], A_0 in $[-15, 15]$ TeV, which are common universal parameters for both the MSSM and the BLSSM, while for the BLSSM we also required $\tan\beta'$ in the interval [0, 2] with neutrino Yukawa couplings $Y^{(1,1)}$, $Y^{(2,2)}$, $Y^{(3,3)}$ in [0, 1]. The $M_{Z'}$ value has been fixed to 4 TeV as discussed in Sec. IV. We will now compare the FT for both the MSSM and BLSSM, using both low- and high-scale parameters.

We begin by presenting a measure of how the SUSY-FT parameter varies with μ in the BLSSM. Figure 6 displays how the SUSY FT parameter, Δ_{SUSY} varies with μ. The FT measure is equal to the maximum contribution from any of the SUSY parameters, but here we see all data points centered on the curve. The tightness of this line (very few points that lie above or below the μ line) shows that very rarely are the other $(m_{h_u}, m_{h_d}, \Sigma_u, \Sigma_d)$ parameters ever responsible for the FT. This behavior is expected, as one can see from the histogram plot of SUSY parameters; see Fig. 5. The corresponding plot for the MSSM looks very

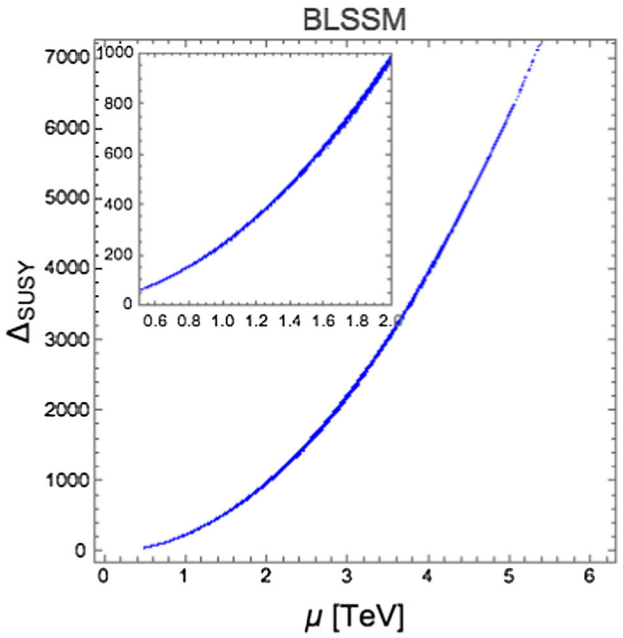

FIG. 6. The SUSY-FT, Δ_{SUSY} vs μ plotted for BLSSM spectrum points. As one expects from Fig. 5, there is a strong dependence of the overall FT, Δ_{SUSY} with the μ parameter; as for nearly every spectrum point, C_μ is the largest of all C parameters.

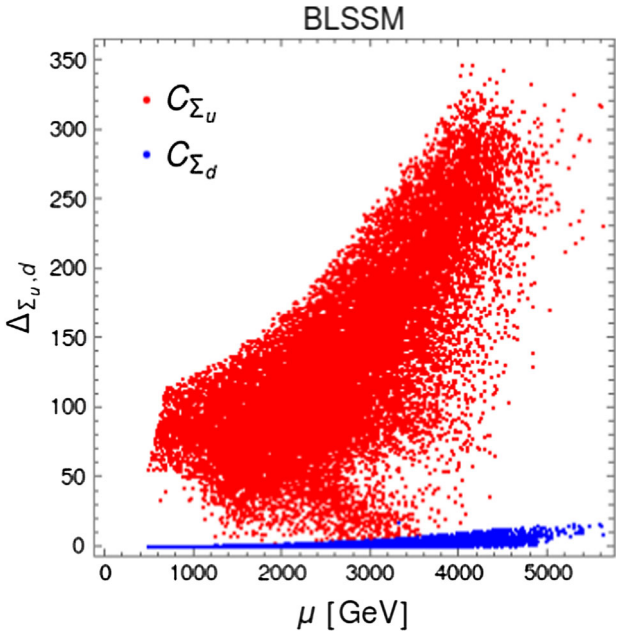

FIG. 7. Strength of loop factors, $\Sigma_{u,d}$, appearing in Eq. (5.11) as a function of μ plotted for BLSSM spectrum points. This may be compared to the overall FT value, appearing in Fig. 6, and one can see the loop factors contributions are never dominant and so loop corrections do not affect the SUSY-FT.

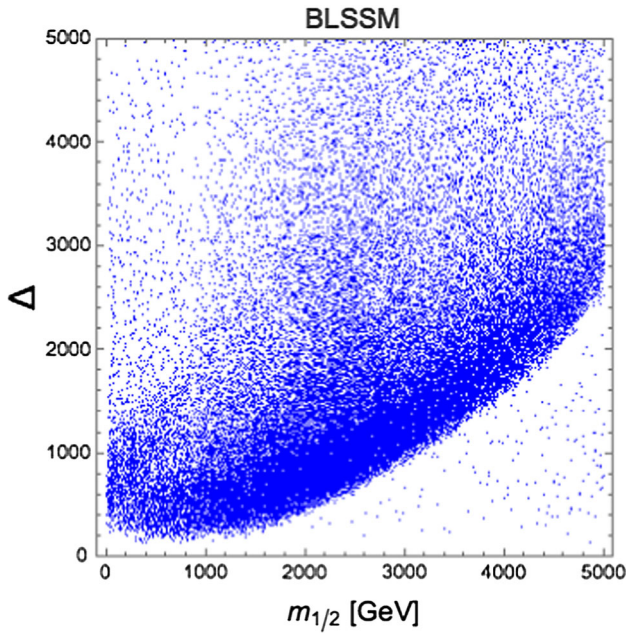

FIG. 8. GUT-FT plotted against $m_{1/2}$ for BLSSM spectrum points. There is a strong dependence for the GUT-FT with the $m_{1/2}$ parameter, although the wide upward spread indicates other parameters may also be the dominant FT contribution.

similar and so is not shown. The behavior is almost identical, as is expected from the MSSM version of the histogram discussed in Sec. V, where the μ parameter dominates the FT.

Now, we turn our attention to considering loop contributions in the SUSY-scale FT. By treating the loop factors as independent parameters which contribute to FT, we may observe their contributions. Figure 7 presents the contribution to FT from Σ_u and Σ_d whilst varying μ. Immediately, one can compare the typical FT values with that of the overall FT as in Fig. 6 and see that the loop contributions will never be the dominant contribution for the FT. There is some growth with μ, but for any given value, the contribution from μ itself is 10 times larger. Since only the maximum contribution of any C_i parameter is taken, we find that treating the tadpole loop contributions as independent of the VEV causes the one-loop FT to look much the same as at tree-level. Once again, this behavior is mimicked in the MSSM, where the VEV independent tadpole loop corrections are also dwarfed by μ's FT.

Penultimately, before we turn to our final comparison of FT, we will discuss the dominant parameters in the GUT-FT sector. Figure 8 shows how the GUT-FT depends on $m_{1/2}$. There is a proportionality with $m_{1/2}$, favoring lower values for a better FT, but the points are not tightly constrained, unlike in SUSY-FT. The upward spread of points indicates that other parameters in addition to $m_{1/2}$ affect the FT. This is expected from the histogram in Fig. 4, where no one single parameter always determines FT, but rather a more even mix.

Finally, in Fig. 9, we will consider how the FT changes in the plane of $(m_0, m_{1/2})$. These parameters have been chosen as they dominantly characterize the behavior of the model itself at the GUT scale. The μ parameter that dominates FT is determined by the minimization conditions, which may be written as functions of m_0 and $m_{1/2}$. We color the points with their FT values in four intervals, namely: red for FT >5000, green for $1000 < \mathrm{FT} < 5000$, orange for $500 < \mathrm{FT} < 1000$ and blue (the least finely tuned points) for $\mathrm{FT} < 500$. The same set of points is used to compare the GUT-FT and the SUSY-FT (there is only a recoloring of these data points between left and right hand side) for the BLSSM and MSSM. The overall picture is similar for all four cases, and it is immediately clear that the FT is comparable between the BLSSM and the MSSM. There is a difference in the distribution of points between the MSSM and BLSSM, where there seem to be no viable points until $m_0 \sim 1$ TeV in the latter. This is due to the requirement of a Z' mass consistent with current constraints (see Sec. IV). Moreover, due to the tadpole equation given in Eq. (1.3) relating $M_{Z'}$ to the soft-masses $m_{\eta_{1,2}}$, which are functions of m_0, notice that a larger $M_{Z'}$ leads to a larger m_0. All four graphs have a similar FT distribution, where a low $m_{1/2}$ is favored and which manifests an approximate independence of m_0. Indeed, $m_{1/2}$ is mostly responsible for the FT rather than m_0 (see Fig. 4). Since there is a little dependence on m_0, we expect to see an increasing FT as $m_{1/2}$ increases, as

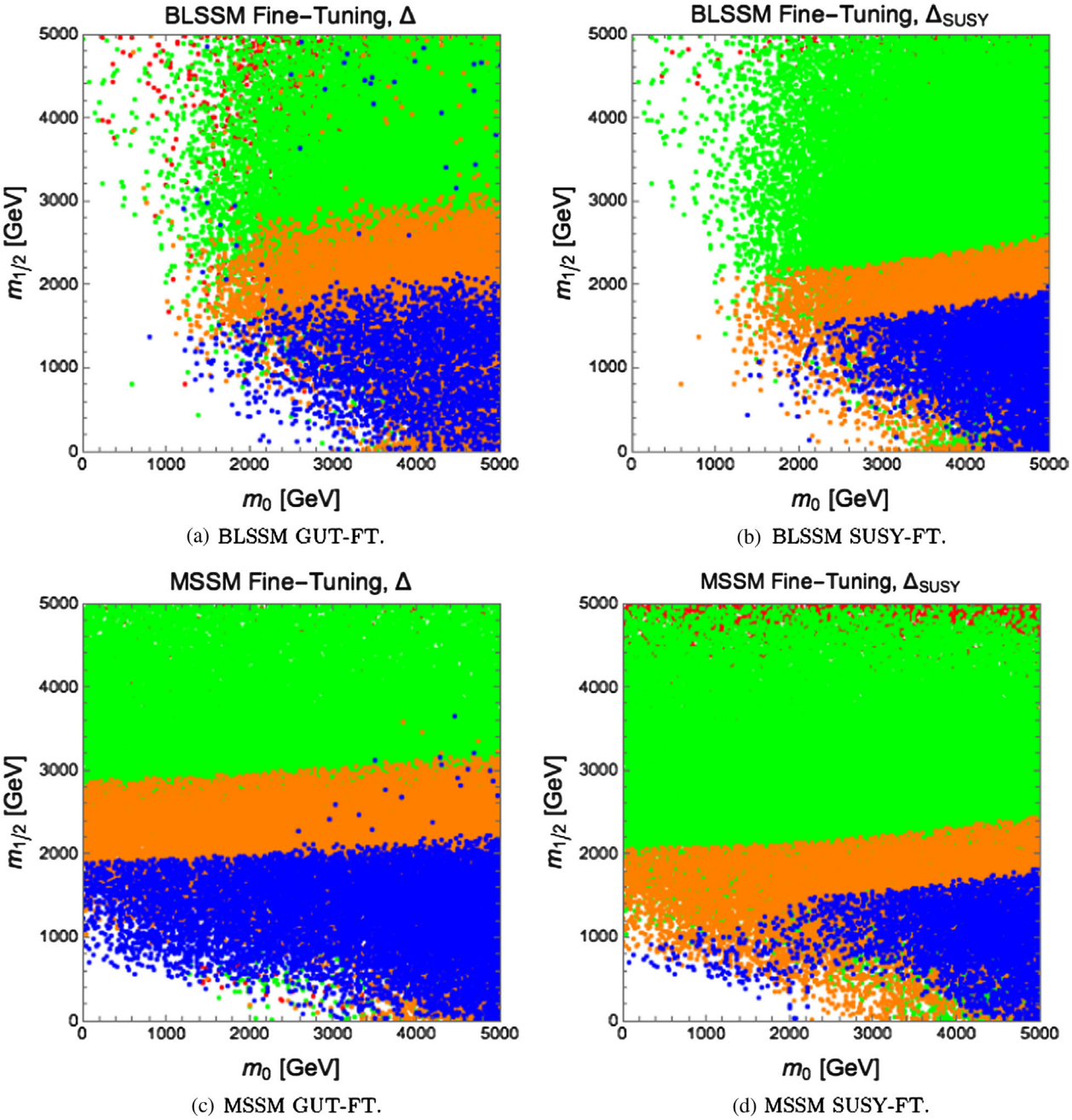

(a) BLSSM GUT-FT. (b) BLSSM SUSY-FT.

(c) MSSM GUT-FT. (d) MSSM SUSY-FT.

FIG. 9. Fine-tuning in the plane of unification of scalar, gaugino masses for BLSSM and MSSM for both GUT-parameters (Δ) and EW parameters (Δ_{EW}). The FT is indicated by the color of the dots: blue for FT < 500; Orange for $500 <$ FT < 1000; Green for $1000 <$ FT < 5000; and Red for FT > 5000.

can be seen in all four cases. When comparing the BLSSM and MSSM GUT-FT, the two pictures are very similar, with a slightly better FT in the MSSM, though the less fine-tuned (blue) points appear about the same mass of $m_{1/2} \approx 2$ TeV. This behavior is very similar when comparing the SUSY-FT between BLSSM and MSSM, where the pictures (up to the distribution of points) are very similar, with a slight dependence on m_0, where larger values are favored. Lastly, we compare the GUT-FT and SUSY-FT for each of the models. In the BLSSM, we find a more concentrated region of less fine-tuned points at higher m_0. Both measures show a strong dependence on $m_{1/2}$. In the MSSM, we again find this dependence, but not the increase in density of less finely tuned points as in the BLSSM. To conclude the discussion on FT, we find that the overall FT is very comparable between the BLSSM and MSSM. Though the GUT-parameter measure is similar in both pictures, with the MSSM as slightly less finely tuned, the BLSSM has a larger density of less finely tuned points when considering SUSY-parameters.

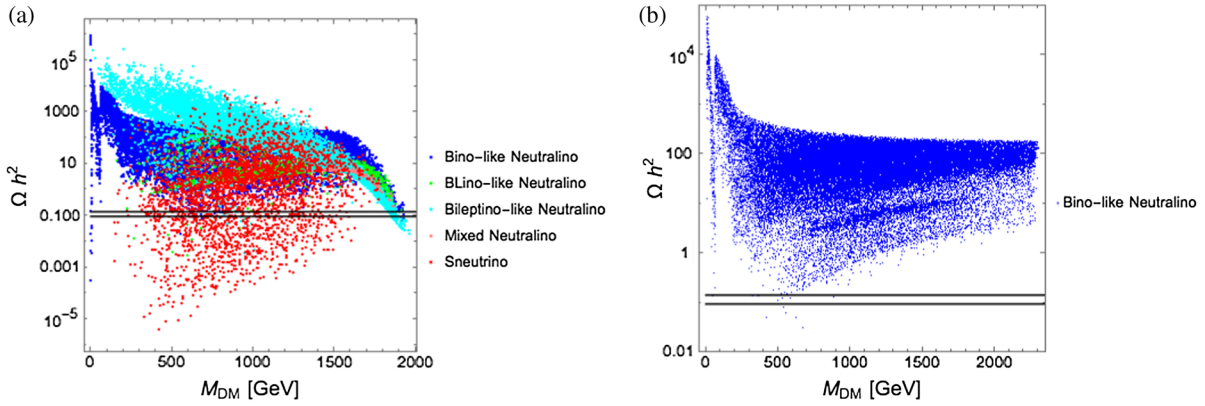

FIG. 10. (a) Relic density vs LSP mass for the BLSSM. (b) Relic density vs LSP mass for the MSSM. In both plots the horizontal lines identify the 2σ region around the current central value of Ωh^2.

We now turn to considering the DM sectors of both models. We will see that once cosmological and direct detection bounds are imposed on the DM candidates, the BLSSM parameter space is far less constrained than the MSSM one, although at the cost of an increased GUT-FT.

For each generated spectrum, the LSP must comply with the cosmological and direct detection bounds of Sec. IV. The relic density in respect to the mass of the LSP ($M_{\rm DM}$) is plotted in Fig. 10(a). The relic is overabundant for the large part of points surviving the screening from collider constraints. Without specifying initial conditions, as those igniting a favorable coannihilation, our scan reveals multiple extended areas with relic densities close to zero. Interestingly, the BLSSM successfully accommodates values within the allowed interval in Eq. (4.1), with all LSP species. The corresponding distributions in Fig. 10(a) have recognizable shapes, which point to different areas where a given LSP is more likely to cross the experimentally allowed interval. Neutralinos may be found mostly, but not entirely, at large $M_{\rm DM}$ values. Sneutrinos appear in a cloud, with low relic density values around the center of our mass span. The sneutrino option stands out as a very promising one, compensating its low rate of production as a LSP with a milder value of the relic with respect to the neutralino.

The extended particle spectrum of the BLSSM yields a more varied nature of the LSP, with more numerous combinations of DM annihilation diagrams, and can play a significant role in dramatically changing the response of the model to the cosmological data, in comparison to the much constrained MSSM. This is well manifested by the relic density computed in the MSSM, as shown in Fig. 10(b). From here, it is obvious how the BLSSM offers a variety of solutions to saturate the relic abundance compatible with the constraints, whether taken at 2σ from the central value measured by experiment or as an absolute upper limit, precluded to the MSSM. In the former, different DM incarnations (bino-, BLino-, bileptinolike and mixed neutralino, alongside the sneutrino) can comply with experimental evidence over a $M_{\rm DM}$ interval which extends up to 2 TeV or so, while in the MSSM case solutions can only be found for much lighter LSP masses and limitedly to one nature (the usual binolike neutralino). Together with the limit on the cosmological relic produced at decoupling by the candidate DM particle, we challenge the constrained BLSSM against the negative search for Weakly Interactive Massive Particle (WIMP) nuclear recoils by the LUX experiment.

The 2016 results of the LUX Collaboration have seen the upper bound on the cross section decreasing by a factor of four in the three years of exposure. Such constraining analyses are still ongoing and will interestingly become a threat or a confirmation of the WIMP hypothesis in future years. From Fig. 11, we notice how the BLSSM with the parameter space investigated largely survives such tight limits. We impose the modified constraint [84]:

$$\sigma_{\rm SI} < \xi \sigma_{\rm SI}^{\rm LUX} \tag{6.1}$$

where

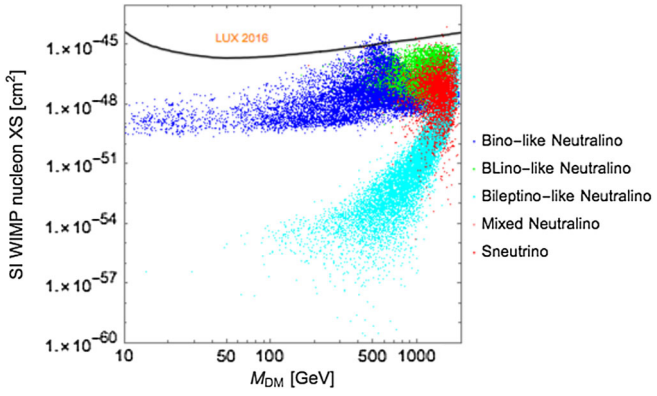

FIG. 11. Spin-independent WIMP-nucleus scattering cross section generated in our scan against the upper bounds from 2016 run of the LUX experiment.

$$\xi = \begin{cases} 1 & \text{if } 0.1168 < \Omega h^2 < 0.1208, \\ \frac{0.1188}{\Omega h^2} & \text{if } \Omega h^2 < 0.1168. \end{cases} \quad (6.2)$$

This accounts for the LUX experimental search assuming the DM has the correct relic density. The effect is to weaken constraints for low relic density points. The LUX bounds have just started touching the BLSSM parameter space, so the next improvements of direct DM searches will continue to further probe BLSSM's parameter space. Even without accounting for this "low relic-density" effect, the picture is still similar. For the MSSM, the SI bounds look identical to the BLSSM, but with a binolike neutralino only.

VII. CONCLUSIONS

While several studies of the SUSY version of the $B-L$ model, BLSSM for short, exist for its low-energy phenomenology and predict distinctive experimental signatures, very little had been said about the theoretical degree of FT required in this scenario in order to produce them. Alternatively, these studies fail to escape current experimental constraints coming from EWPOs, collider and cosmological data. We have addressed these issues in the first part of this paper, by adopting a suitable FT measure amongst those available in literature and expressed it in terms of the low-energy spectra of the MSSM and BLSSM as well as of the (high-scale) universal parameters of the two models. The latter, for the MSSM, include masses for scalars and gauginos, trilinear coupling, Higgsino mass and the quadratic soft SUSY term. In the BLSSM, we have all of these parameters plus two additional ones, the BLino mass and another quadratic soft SUSY term. The low- and high-energy spectra in the two SUSY scenarios can be related by RGEs, which we have computed numerically at two-loop level.

We have found that the level of FT required in the BLSSM is somewhat higher than in the MSSM when computed at the GUT scale in presence of all available experimental constraints, but those connected to DM searches, and this is primarily driven by the requirement of a large Z' mass, of order 4 TeV or higher, which in turn corresponds to somewhat different acceptable values for the scalar and fermionic unification masses, which partially reflect in different low-energy spectra potentially accessible at the LHC. However, when the FT is computed at the SUSY scale, the pull now originating from all available experimental constraints, chiefly the DM ones, destabilizes the MSSM more than the BLSSM, as the latter appears more natural, well reflecting a much lower level of tension against data existing in the latter with respect to the former.

Furthermore, we have examined the response to the relic density constraints of the nonminimal SUSY scenario, wherein the extra $B-L$ neutralinos (three extra neutral fermions, i.e., a $U(1)_{B-L}$ gaugino $\tilde{B}'$ and two extra Higgsinos $\tilde{\eta}$) can be cold DM candidates. As well known, taking the lightest neutralino in the MSSM as the sole possible DM candidate implies severe constraints on the parameter space of this scenario. Indeed, in the case of universal soft-breaking terms, the MSSM is almost ruled out by combining collider, astrophysics and rare decay constraints. Therefore, it is important to explore very well motivated extensions of the MSSM, such as the BLSSM, that provide new DM candidates that may account for the relic density with no conflict with other phenomenological constraints.

After an extensive study in this direction, we have concluded that the extended particle spectrum of the BLSSM, in turn translating into a more varied nature of the LSP as well as a more numerous combination of DM annihilation diagrams, can play a significant role in dramatically changing the ability of SUSY to adapt to cosmological data, in comparison to the much constrained MSSM. In fact, the BLSSM offers a variety of solutions to the relic abundance constraint, whether taken at 2σ from the central value measured by experiment or as an absolute upper limit, which are unavailable in the MSSM. Alongside the usual bino- (and possibly sneutrino), the BLino- and bileptinolike as well as the mixed neutralino can comply with experimental evidence over an M_{DM} interval which extends up to 2 TeV or so, while in the MSSM case solutions can only be found for much lighter LSP masses ($\sim$500 GeV) and limited to the standard binolike neutralino.

ACKNOWLEDGMENTS

S. M. is supported in part through the NExT Institute. The work of L. D. R. has been supported by the "Angelo Della Riccia" foundation and the STFC/COFUND Rutherford International Fellowship scheme. The work of C. M. is supported by the "Angelo Della Riccia" foundation and by the Centre of Excellence Project No. TK133, Dark Side of the Universe. The work of S. K. is partially supported by the STDF Project No. 13858. All authors acknowledge support from the Grant H2020-MSCA-RISE-2014 No. 645722 (NonMinimalHiggs).

APPENDIX: BLSSM β FUNCTION COEFFICIENTS

We complete the list of the β functions giving those concerning the soft masses of the scalar fields H_u, H_d and η_1, η_2. These are given, at one loop, by

$$\beta_{m^2_{H_u}} = -\frac{6}{5}(g_1^2(M_1^2+\tilde{M}^2)+\tilde{g}^2(M_1'^2+\tilde{M}^2)+2g_1\tilde{g}(M_1+M_1')\tilde{M})-6g_2^2M_W^2,$$
$$-3(g_1^2+\tilde{g}^2)\sigma_1-\frac{3\sqrt{10}}{4}g_{BL}\tilde{g}\sigma_2+6(m^2_{H_u}+m^2_{q_{33}}+m^2_{u_{33}})Y_t^2+6T_t^2 \quad \text{(A1)}$$

$$\beta_{m^2_{H_d}} = -\frac{6}{5}(g_1^2(M_1^2+\tilde{M}^2)+\tilde{g}^2(M_1'^2+\tilde{M}^2)+2g_1\tilde{g}(M_1+M_1')\tilde{M})-6g_2^2M_W^2,$$
$$+3(g_1^2+\tilde{g}^2)\sigma_1+\frac{3\sqrt{10}}{4}g_{BL}\tilde{g}\sigma_2+6(m^2_{H_d}+m^2_{q_{33}}+m^2_{d_{33}})Y_b^2+6T_b^2 \quad \text{(A2)}$$

$$\beta_{m^2_{\eta_1}} = -12{g_{BL}}^2(M_1'^2+\tilde{M}^2)+4m^2_{\eta_1}\mathrm{tr}(Y_N^2)+4\mathrm{tr}(T^2_{Y_N})+8\mathrm{tr}(m^2_{\nu_R}Y_N^2),+3\sqrt{\frac{2}{5}}g_{BL}\tilde{g}\sigma_1+\frac{3}{2}{g_{BL}}^2\sigma_2, \quad \text{(A3)}$$

$$\beta_{m^2_{\eta_2}} = -12{g_{BL}}^2(M_1'^2+\tilde{M}^2)-3\sqrt{\frac{2}{5}}g_{BL}\tilde{g}\sigma_1-\frac{3}{2}{g_{BL}}^2\sigma_2, \quad \text{(A4)}$$

where, for the sake of simplicity, we have neglected all the Yukawa couplings but top- and bottom-quark Y_t, Y_b and the heavy-neutrinos Y_N. We have also assumed real parameters.

[1] A. M. Sirunyan *et al.* (CMS Collaboration), Search for supersymmetry in multijet events with missing transverse momentum in proton-proton collisions at 13 TeV, arXiv:1704.07781; The ATLAS Collaboration (ATLAS Collaboration), Report No. ATLAS-CONF-2017-021.

[2] See, for instance, P. Bechtle *et al.*, Killing the cMSSM softly, Eur. Phys. J. C **76**, 96 (2016), and references therein.

[3] H. Baer, V. Barger, D. Mickelson, and M. Padeffke-Kirkland, SUSY models under siege: LHC constraints and electroweak fine-tuning, Phys. Rev. D **89**, 115019 (2014).

[4] D. S. Akerib *et al.* (LUX Collaboration), Results on the Spin-Dependent Scattering of Weakly Interacting Massive Particles on Nucleons from the Run 3 Data of the LUX Experiment, Phys. Rev. Lett. **116**, 161302 (2016).

[5] W. Abdallah and S. Khalil, MSSM dark matter in light of Higgs and LUX results, Adv. High Energy Phys. **2016** (2016) 5687463; Q. Shafi, Ś. H. Tanyıldızı, and C. S. Un, Neutralino dark matter and other LHC predictions from quasi Yukawa unification, Nucl. Phys. **B900**, 400 (2015); A. Hebbar, Q. Shaf,i, and C. S. Un, Light Higgsinos, heavy gluino, and $b-\tau$ quasi-Yukawa unification: Prospects for finding the gluino at the LHC, Phys. Rev. D **95**, 115026 (2017).

[6] G. Hinshaw *et al.* (WMAP Collaboration), Nine-Year Wilkinson Microwave Anisotropy Probe (WMAP) Observations: Cosmological parameter results, Astrophys. J. Suppl. Ser. **208**, 19 (2013).

[7] P. A. R. Ade *et al.* (Planck Collaboration), Planck 2015 results. XIII. Cosmological parameters, Astron. Astrophys. **594**, A13 (2016).

[8] S. Khalil, Low scale $B-L$ extension of the Standard Model at the LHC, J. Phys. G **35**, 055001 (2008).

[9] L. Basso, A. Belyaev, S. Moretti, and C. H. Shepherd-Themistocleous, Phenomenology of the minimal B-L extension of the Standard model: Z' and neutrinos, Phys. Rev. D **80**, 055030 (2009).

[10] L. Basso, A. Belyaev, S. Moretti, G. M. Pruna, and C. H. Shepherd-Themistocleous, Phenomenology of the minimal $B-L$ extension of the Standard Model, *Proc. Sci.*, EPS-HEP2009 (2009) 242 [arXiv:0909.3113].

[11] L. Basso, S. Moretti, and G. M. Pruna, Phenomenology of the minimal $B-L$ extension of the Standard Model: the Higgs sector, Phys. Rev. D **83**, 055014 (2011).

[12] L. Basso, A. Belyaev, S. Moretti, and G. M. Pruna, Higgs phenomenology in the minimal $B-L$ extension of the Standard Model at LHC, J. Phys. Conf. Ser. **259**, 012062 (2010).

[13] S. K. Majee and N. Sahu, Dilepton Signal of a type-II seesaw at CERN LHC: Reveals a TeV scale B-L symmetry, Phys. Rev. D **82**, 053007 (2010).

[14] T. Li and W. Chao, Neutrino Masses, Dark Matter and B-L Symmetry at the LHC, Nucl. Phys. **B843**, 396 (2011).

[15] P. Fileviez Perez, T. Han, and T. Li, Testability of type I seesaw at the CERN LHC: Revealing the existence of the B-L symmetry, Phys. Rev. D **80**, 073015 (2009).

[16] W. Emam and S. Khalil, Higgs and Z-prime phenomenology in B-L extension of the standard model at LHC, Eur. Phys. J. C **52**, 625 (2007).

[17] S. Khalil and S. Moretti, Heavy neutrinos, Z' and Higgs bosons at the LHC: New particles from an old symmetry, J. Mod. Phys. **4**, 26697 (2013).

[18] S. Khalil and S. Moretti, A simple symmetry as a guide toward new physics beyond the Standard Model, Front. Phys. **1**, 10 (2013).

[19] S. Khalil, Radiative symmetry breaking in supersymmetric $B-L$ models with an inverse seesaw mechanism, Phys. Rev. D **94**, 075003 (2016).

[20] S. Khalil and A. Masiero, Radiative B-L symmetry breaking in supersymmetric models, Phys. Lett. B **665**, 374 (2008).

[21] P. Fileviez Perez and S. Spinner, The fate of R-parity, Phys. Rev. D **83**, 035004 (2011).

[22] J. E. Camargo-Molina, B. O'Leary, W. Porod, and F. Staub, The stability of R-parity In supersymmetric models extended by $\mathrm{U}(1)_{B-L}$, Phys. Rev. D **88**, 015033 (2013).

[23] T. Kikuchi and T. Kubo, Radiative B-L symmetry breaking and the Z-prime mediated SUSY breaking, Phys. Lett. B **666**, 262 (2008).

[24] R. M. Fonseca, M. Malinsky, W. Porod, and F. Staub, Running soft parameters in SUSY models with multiple U(1) gauge factors, Nucl. Phys. **B854**, 28 (2012).

[25] A. Elsayed, S. Khalil, and S. Moretti, Higgs mass corrections in the SUSY B-L model with inverse seesaw, Phys. Lett. B **715**, 208 (2012).

[26] L. Basso and F. Staub, Enhancing $h \to \gamma\gamma$ with staus in SUSY models with extended gauge sector, Phys. Rev. D **87**, 015011 (2013).

[27] B. O'Leary, W. Porod, and F. Staub, Mass spectrum of the minimal SUSY B-L model, J. High Energy Phys. 05 (2012) 042.

[28] L. Basso, A. Belyaev, D. Chowdhury, M. Hirsch, S. Khalil, S. Moretti, B. O'Leary, W. Porod, and F. Staub, Proposal for generalised Supersymmetry Les Houches Accord for seesaw models and PDG numbering scheme, Comput. Phys. Commun. **184**, 698 (2013).

[29] A. Elsayed, S. Khalil, S. Moretti, and A. Moursy, Right-handed sneutrino-antisneutrino oscillations in a TeV scale Supersymmetric B-L model, Phys. Rev. D **87**, 053010 (2013).

[30] S. Khalil and S. Moretti, The $B-L$ supersymmetric standard model with inverse seesaw at the Large Hadron Collider, Rep. Prog. Phys. **80**, 036201 (2017).

[31] W. Abdallah, S. Khalil, and S. Moretti, Double Higgs peak in the minimal SUSY B-L model, Phys. Rev. D **91**, 014001 (2015).

[32] L. Basso, B. O'Leary, W. Porod, and F. Staub, Dark matter scenarios in the minimal SUSY B-L model, J. High Energy Phys. 09 (2012) 054.

[33] W. Abdallah, J. Fiaschi, S. Khalil, and S. Moretti, Z'-induced invisible right-handed sneutrino decays at the LHC, Phys. Rev. D **92**, 055029 (2015).

[34] W. Abdallah, J. Fiaschi, S. Khalil, and S. Moretti, Mono-jet, -photon and -Z signals of a supersymmetric (B—L) model at the Large Hadron Collider, J. High Energy Phys. 02 (2016) 157.

[35] A. Hammad, S. Khalil, and S. Moretti, LHC signals of a B-L supersymmetric standard model CP -even Higgs boson, Phys. Rev. D **93**, 115035 (2016).

[36] A. Hammad, S. Khalil, and S. Moretti, Higgs boson decays into $\gamma\gamma$ and $Z\gamma$ in the MSSM and the B-L supersymmetric SM, Phys. Rev. D **92**, 095008 (2015).

[37] R. Barbieri and A. Strumia, About the fine tuning price of LEP, Phys. Lett. B **433**, 63 (1998).

[38] G. Cacciapaglia, C. Csaki, G. Marandella, and A. Strumia, The minimal set of electroweak precision parameters, Phys. Rev. D **74**, 033011 (2006).

[39] R. Wendell *et al.* (Super-Kamiokande collaboration), Atmospheric neutrino oscillation analysis with sub-leading effects in Super-Kamiokande I, II, and III, Phys. Rev. D **81**, 092004 (2010).

[40] C. S. Aulakh, A. Melfo, A. Rasin, and G. Senjanovic, Seesaw and supersymmetry or exact R-parity, Phys. Lett. B **459**, 557 (1999).

[41] B. Holdom, Two U(1)'s and epsilon charge shifts, Phys. Lett. B **166**, 196 (1986).

[42] S. Khalil and C. S. Un, Muon anomalous magnetic moment in SUSY $B-L$ model with inverse seesaw, Phys. Lett. B **763**, 164 (2016).

[43] C. Coriano, L. Delle Rose, and C. Marzo, Constraints on abelian extensions of the Standard Model from two-loop vacuum stability and $U(1)_{B-L}$, J. High Energy Phys. 02 (2016) 135.

[44] F. Staub, SARAH 4: A tool for (not only SUSY) model builders, Comput. Phys. Commun. **185**, 1773 (2014).

[45] W. Porod, SPheno, a program for calculating supersymmetric spectra, SUSY particle decays and SUSY particle production at $e^+ e^-$ colliders, Comput. Phys. Commun. **153**, 275 (2003).

[46] E. Accomando, C. Coriano, L. Delle Rose, J. Fiaschi, C. Marzo, and S. Moretti, Z', Higgses and heavy neutrinos in U(1)' models: from the LHC to the GUT scale, J. High Energy Phys. 07 (2016) 086.

[47] V. Khachatryan *et al.* (CMS collaboration), Search for narrow resonances in dilepton mass spectra in proton-proton collisions at $\sqrt{s} = 13$ TeV and combination with 8 TeV data, Phys. Lett. B **768**, 57 (2017).

[48] P. Bechtle, O. Brein, S. Heinemeyer, G. Weiglein, and K. E. Williams, HiggsBounds: Confronting Arbitrary Higgs Sectors with Exclusion Bounds from LEP and the Tevatron, Comput. Phys. Commun. **181**, 138 (2010).

[49] P. Bechtle, O. Brein, S. Heinemeyer, G. Weiglein, and K. E. Williams, HiggsBounds 2.0.0: Confronting Neutral and Charged Higgs Sector Predictions with Exclusion Bounds from LEP and the Tevatron, Comput. Phys. Commun. **182**, 2605 (2011).

[50] P. Bechtle, O. Brein, S. Heinemeyer, O. Stål, T. Stefaniak, G. Weiglein, and K. E. Williams, HiggsBounds-4: Improved Tests of Extended Higgs Sectors against Exclusion Bounds from LEP, the Tevatron and the LHC, Eur. Phys. J. C **74**, 2693 (2014).

[51] P. Bechtle, S. Heinemeyer, O. Stål, T. Stefaniak, and G. Weiglein, Applying exclusion likelihoods from LHC searches to extended Higgs sectors, Eur. Phys. J. C **75**, 421 (2015).

[52] P. Bechtle, S. Heinemeyer, O. Stål, T. Stefaniak, and G. Weiglein, HiggsSignals: Confronting arbitrary Higgs sectors with measurements at the Tevatron and the LHC, Eur. Phys. J. C **74**, 2711 (2014).

[53] K. A. Olive *et al.* (Particle Data Group Collaboration), Review of particle physics, Chin. Phys. C **38**, 090001 (2014).

[54] G. Belanger, F. Boudjema, A. Pukhov, and A. Semenov, MicrOMEGAs 2.0: A Program to calculate the relic density

of dark matter in a generic model, Comput. Phys. Commun. **176**, 367 (2007).
[55] G. Belanger, F. Boudjema, A. Pukhov, and A. Semenov, micrOMEGAs$_3$: A program for calculating dark matter observables, Comput. Phys. Commun. **185**, 960 (2014).
[56] D. S. Akerib *et al.*, Results from a Search for Dark Matter in the Complete LUX Exposure, Phys. Rev. Lett. **118**, 021303 (2017).
[57] T. Falk, K. A. Olive, and M. Srednicki, Heavy sneutrinos as dark matter, Phys. Lett. B **339**, 248 (1994).
[58] G. W. Anderson and D. J. Castano, Measures of fine tuning, Phys. Lett. B **347**, 300 (1995).
[59] G. W. Anderson and D. J. Castano, Naturalness and superpartner masses or when to give up on weak scale supersymmetry, Phys. Rev. D **52**, 1693 (1995).
[60] G. W. Anderson and D. J. Castano, Challenging weak scale supersymmetry at colliders, Phys. Rev. D **53**, 2403 (1996).
[61] G. W. Anderson, D. J. Castano, and A. Riotto, Naturalness lowers the upper bound on the lightest Higgs boson mass in supersymmetry, Phys. Rev. D **55**, 2950 (1997).
[62] P. Ciafaloni and A. Strumia, Naturalness upper bounds on gauge mediated soft terms, Nucl. Phys. **B494**, 41 (1997).
[63] K. L. Chan, U. Chattopadhyay, and P. Nath, Naturalness, weak scale supersymmetry and the prospect for the observation of supersymmetry at the Tevatron and at the CERN LHC, Phys. Rev. D **58**, 096004 (1998).
[64] L. Giusti, A. Romanino, and A. Strumia, Natural ranges of supersymmetric signals, Nucl. Phys. **B550**, 3 (1999).
[65] J. A. Casas, J. R. Espinosa, and I. Hidalgo, The MSSM fine tuning problem: A Way out, J. High Energy Phys. 01 (2004) 008.
[66] J. A. Casas, J. R. Espinosa, and I. Hidalgo, A Relief to the supersymmetric fine tuning problem, in *String phenomenology. Proceedings, 2nd International Conference, Durham, UK, 2003* (2004), p. 76 [arXiv:hep-ph/0402017].
[67] J. A. Casas, J. R. Espinosa, and I. Hidalgo, Implications for new physics from fine-tuning arguments. 1. Application to SUSY and seesaw cases, J. High Energy Phys. 11 (2004) 057.
[68] J. A. Casas, J. R. Espinosa, and I. Hidalgo, Expectations for LHC from naturalness: modified versus SM Higgs sector, Nucl. Phys. **B777**, 226 (2007).
[69] R. Kitano and Y. Nomura, A solution to the supersymmetric fine-tuning problem within the MSSM, Phys. Lett. B **631**, 58 (2005).
[70] P. Athron and D. J. Miller, A new measure of fine tuning, Phys. Rev. D **76**, 075010 (2007).
[71] H. Baer, V. Barger, P. Huang, A. Mustafayev, and X. Tata, Radiative Natural SUSY with a 125 GeV Higgs Boson, Phys. Rev. Lett. **109**, 161802 (2012).
[72] J. R. Ellis, K. Enqvist, D. V. Nanopoulos, and F. Zwirner, Aspects of the superunification of strong, electroweak and gravitational interactions, Nucl. Phys. **B276**, 14 (1986).
[73] R. Barbieri and G. F. Giudice, Upper bounds on supersymmetric particle masses, Nucl. Phys. **B306**, 63 (1988).
[74] G. G. Ross, K. Schmidt-Hoberg, and F. Staub, Revisiting fine-tuning in the MSSM, J. High Energy Phys. 03 (2017) 021.
[75] H. Baer, V. Barger, P. Huang, and X. Tata, Natural supersymmetry: LHC, dark matter and ILC searches, J. High Energy Phys. 05 (2012) 109.
[76] H. Baer, V. Barger, P. Huang, D. Mickelson, A. Mustafayev, and X. Tata, Radiative natural supersymmetry: Reconciling electroweak fine-tuning and the Higgs boson mass, Phys. Rev. D **87**, 115028 (2013).
[77] M. W. Cahill-Rowley, J. L. Hewett, A. Ismail, and T. G. Rizzo, Higgs sector and fine-tuning in the phenomenological MSSM, Phys. Rev. D **86**, 075015 (2012).
[78] J. L. Feng and D. Sanford, A Natural 125 GeV Higgs Boson in the MSSM from Focus Point Supersymmetry with A-Terms, Phys. Rev. D **86**, 055015 (2012).
[79] Z. Kang, J. Li, and T. Li, On naturalness of the MSSM and NMSSM, J. High Energy Phys. 11 (2012) 024.
[80] H. Baer, V. Barger, and D. Mickelson, How conventional measures overestimate electroweak fine-tuning in supersymmetric theory, Phys. Rev. D **88**, 095013 (2013).
[81] H. Baer, V. Barger, and D. Mickelson, Direct and indirect detection of higgsino-like WIMPs: concluding the story of electroweak naturalness, Phys. Lett. B **726**, 330 (2013).
[82] K. Kowalska and E. M. Sessolo, Natural MSSM after the LHC 8 TeV run, Phys. Rev. D **88**, 075001 (2013).
[83] The ATLAS Collaboration, Report No. ATLAS-CONF-2015-067, 2015.
[84] G. Belanger, D. Ghosh, R. Godbole, and S. Kulkarni, Light stop in the MSSM after LHC Run 1, J. High Energy Phys. 09 (2015) 214.